PCCP

Cite this: *Phys. Chem. Chem. Phys.*, 2012, **14**, 10424–10437

www.rsc.org/pccp

PAPER

Reaction dynamics of CN radicals with tetrahydrofuran in liquid solutions†

R. A. Rose,‡[a] S. J. Greaves,[a] F. Abou-Chahine,[a] D. R. Glowacki,*[a] T. A. A. Oliver,§[a] M. N. R. Ashfold,[a] I. P. Clark,[b] G. M. Greetham,[b] M. Towrie[b] and A. J. Orr-Ewing*[a]

Received 16th January 2012, Accepted 27th March 2012
DOI: 10.1039/c2cp40158d

Transient, broadband infra-red absorption spectroscopy with picosecond time resolution has been used to study the dynamics of reactions of CN radicals with tetrahydrofuran (THF) and d_8-THF in liquid solutions ranging from neat THF to 0.5 M THF in chlorinated solvents ($CDCl_3$ and CD_2Cl_2). HCN and DCN products were monitored *via* their ν_1 (C≡N stretching) and ν_3 (C−H(D) stretching) vibrational absorption bands. Transient spectral features indicate formation of vibrationally excited HCN and DCN, and the onsets of absorption *via* the fundamental bands of HCN and DCN show short (5–15 ps) delays consistent with vibrational relaxation within the nascent reaction products. This interpretation is confirmed by non-equilibrium molecular dynamics simulations employing a newly derived analytic potential energy surface for the reaction in explicit THF solvent. The rate coefficient for reactive formation of HCN (as determined from measurements on both the 1_0^1 and 3_0^1 fundamental bands) decreases with increasing dilution of the THF in $CDCl_3$ or CD_2Cl_2, showing pseudo-first order kinetic behaviour for THF concentrations in the range 0.5–4.5 M, and a bimolecular rate coefficient of $(1.57 \pm 0.12) \times 10^{10}$ M^{-1} s^{-1} is derived. Simultaneous analysis of time-dependent HCN 1_0^1 and 3_0^1 band intensities following reaction of CN with THF (3.0 M) in CD_2Cl_2 suggests that C−H stretching mode excitation is favoured, and this deduction is supported by the computer simulations. The results extend our recent demonstration of nascent vibrational excitation of the products of bimolecular reactions in liquid solution to a different, and more strongly interacting class of organic solvents. They serve to reinforce the finding that dynamics (and thus the topology of the reactive potential energy surface) play an important role in determining the nascent product state distributions in condensed phase reactions.

1. Introduction

The dynamics of bimolecular chemical reactions have been the subject of extensive experimental and theoretical study for isolated collisions in the gas phase,[1,2] or for collisions of gas phase molecules at solid surfaces,[2] and there is growing interest in reactive scattering from liquid surfaces.[3] However, despite the importance of the liquid phase as a medium for many chemical and biochemical processes, there are very few comparable studies to date of bimolecular reactions in bulk liquid solutions. As we have recently shown, the dynamics of reactions in liquids are amenable to detailed examination on ultrafast timescales,[4] and such studies offer new insights about the microscopic role of the solvent and solute molecules during chemical reactions.[5–7]

In a series of recent studies, we investigated the dynamics of CN radical reactions with organic molecules (cyclohexane, d_{12}-cyclohexane and tetramethylsilane) in solution in the chlorinated solvents chloroform and dichloromethane.[4,7,8] These studies built on picosecond (ps) infra-red (IR) absorption measurements by Hochstrasser and coworkers of the time dependence of formation of products of reactions of CN radicals with chloroform and Cl atoms with cyclohexane,[9,10]

[a] *School of Chemistry, University of Bristol, Cantock's Close, Bristol BS8 1TS, UK. E-mail: a.orr-ewing@bris.ac.uk, david.r.glowacki@bris.ac.uk; Fax: +44 117 9277985; Tel: +44 117 9287672*
[b] *Central Laser Facility, Research Complex at Harwell, Science and Technology Facilities Council, Rutherford Appleton Laboratory, Harwell Science and Innovation Campus, Didcot, Oxfordshire OX11 0QX, UK*

† Electronic supplementary information (ESI) available. See DOI: 10.1039/c2cp40158d

‡ Current address: RAL Space, Science and Technology Facilities Council, Rutherford Appleton Laboratory, Harwell Science and Innovation Campus, Didcot, Oxfordshire, OX11 0QX, UK.
§ Current address: Department of Chemistry, University of California, Berkeley, CA 84720, USA.

and extensive transient IR and ultraviolet (UV) absorption studies by Crim and coworkers of rates of reactions of CN radicals or Cl atoms with various organic solutes in chlorinated solvents.[11–14] In our previous experiments, the vibrational state specific dynamics of formation of HCN (and DCN) were examined using transient broadband IR absorption spectroscopy with ps time resolution. The HCN products of reaction of CN radicals with *c*-C_6H_{12}, for example, were shown to form with preferential excitation of a quantum of the C–H stretching mode and up to two quanta of the bending vibrational mode, followed by relaxation back to the ground state by solvent quenching on characteristic timescales of 130–270 ps.[4,8] Comparison between such solution-phase dynamics and those previously observed for reaction in the gas-phase provides unusual opportunities to learn about the influence exerted by the solvent on fundamental reaction mechanisms.[6,15]

Here, we report the outcomes of a study of CN radical reaction dynamics in tetrahydrofuran (THF, *c*-C_4H_8O) and d_8-THF (*c*-C_4D_8O), in which the THF serves as a representative commonplace but non-halogenated solvent. The cavitied structure of liquid THF, and its role in charge-transfer-to-solvent dynamics, have been the subjects of extensive prior investigations.[16–19] Our focus is on reaction with the solvent by H(D)-atom abstraction:

$$CN + c\text{-}C_4H_8O \rightarrow HCN + c\text{-}C_4H_7O \quad (1)$$

$$CN + c\text{-}C_4D_8O \rightarrow DCN + c\text{-}C_4D_7O \quad (2)$$

for which a combination of experimental measurements and accompanying computer simulations of the reaction dynamics in solution provide detailed mechanistic insights. To unravel the dynamics further, experiments were carried out at a series of dilutions of the THF in a chlorinated solvent selected not to contribute to reactive signals. Reactions were initiated by ~50-fs UV laser photodissociation of ICN present in dilute solution and the HCN or DCN products were probed in absorption over a ~500 cm^{-1} bandwidth in the ν_3 (C−H stretching in HCN and with C−D stretching character in DCN) and ν_1 (C≡N stretching) regions with 1 ps time resolution. Various transient absorption features were observed, and are analysed in combination with vibrational relaxation time constants derived from IR-pump and IR-probe experiments to derive the kinetics and dynamics of formation of vibrationally excited and ground state reaction products. The rapid formation of INC *via* geminate recombination following ICN photodissociation is also reported.

2. Experimental

All experiments were carried out using the ultrafast UV and IR laser capabilities of the ULTRA laser system at the Central Laser Facility of the Rutherford Appleton Laboratory. The laser system and experimental methods have been described in detail elsewhere,[4,20] and only a brief summary is given here. ICN (98%; Acros Organics) samples were prepared as 0.14 M solutions in THF, d_8-THF or solutions of THF in $CDCl_3$ or CD_2Cl_2 (all organic solvents from Sigma-Aldrich, purity typically >99.9%; d_8-THF 99.5 atom%; $CDCl_3$ and CD_2Cl_2 99.96 atom%). The ICN was photolysed by ~50 fs duration UV pulses of wavelength 266 nm, which defined the zero of time in the experiments. The CN radicals from the photodissociation, >98% of which are expected to be in their ground vibrational level,[21] reacted with the THF or recombined to form INC or ICN and the resultant products were probed after an interval of 1–2500 ps (set using an optical delay line) by transient IR absorption using a ~500 cm^{-1} bandwidth IR laser pulse. The IR radiation transmitted by the sample was dispersed onto a pair of 128-pixel arrays from which spectra were captured and averaged at each time delay. Difference spectra were derived from spectra accumulated with and without the UV laser on successive shots. The sample solutions were circulated by a peristaltic pump through a rastered Harrick cell fitted with BaF_2 or CaF_2 windows spaced 0.38 mm apart. The lasers operated at repetition rates of 10 kHz, and cell rastering and rapid circulation ensured there was no build-up of reaction products between IR laser pulses.

Spectra at numerous time delays between the two laser pulses, selected in random order, were normalized to the spectral profile of the probe laser (recorded shot-by-shot on a third array detector) and corrected for any baseline absorption and scattering features. Wavelength calibration of the spectra was achieved by placing a thin sample of 1,4-dioxane in the path of the IR laser (in place of the ICN/THF sample) and recording an absorption spectrum that was compared to an FTIR spectrum of the same sample. The linear pixel to wavelength calibration was followed by a transformation to a wavenumber scale for analysis and presentation of spectra.

HCN and DCN spectral features in solution were identified by exposing a static ICN/THF solution in a Harrick cell to irradiation by the fourth harmonic (266 nm) of a 10 kHz nanosecond Nd : YAG laser for ~20 min, and comparing the FTIR spectra of the sample before and after this irradiation. For HCN, a distinct band was evident with maximum at 2078 cm^{-1}, and is assigned to the C≡N stretching fundamental vibration of HCN, but IR activity in the C−H stretching region was masked by a strong solvent absorption band. Attempts to observe transient HCN absorptions on the shoulder of this strong solvent feature were unsuccessful for neat THF as a solvent, but they could be observed centred at 3259 cm^{-1} (with FWHM of ~25 cm^{-1}) upon dilution in $CDCl_3$ or CD_2Cl_2. Fig. 1 shows FTIR spectra of DCN/d_8-THF and DCN/$CHCl_3$ solutions, with the DCN prepared by UV laser irradiation of ICN/d_8-THF and ICN/d_{12}-cyclohexane/$CHCl_3$ solutions respectively. Taking the difference between sample spectra after and before UV irradiation reveals the DCN bands shown, and these are assigned to fundamental transition of the ν_3 mode. In solution in d_8-THF, the DCN band peaks at 2520 cm^{-1}, compared to 2607 cm^{-1} in $CHCl_3$ and 2630 cm^{-1} in the gas phase,[22] and is notably broadened with a FWHM of ~75 cm^{-1} compared to ~10 cm^{-1} in $CHCl_3$. The shift and broadening of the band indicate strong interaction of the DCN with d_8-THF through the C−D moiety, although there is a suggestion of a shoulder to the band in Fig. 1 at ~2610 cm^{-1} that may reflect an alternative, more weakly solvated environment.

Static solutions comprising HCN in THF, 3.0 M THF in $CDCl_3$, 3.0 M THF in CD_2Cl_2, and DCN in d_8-THF, prepared by 266-nm photolysis of ICN (0.14 M) as described above, were also used in IR-pump and IR-probe experiments to

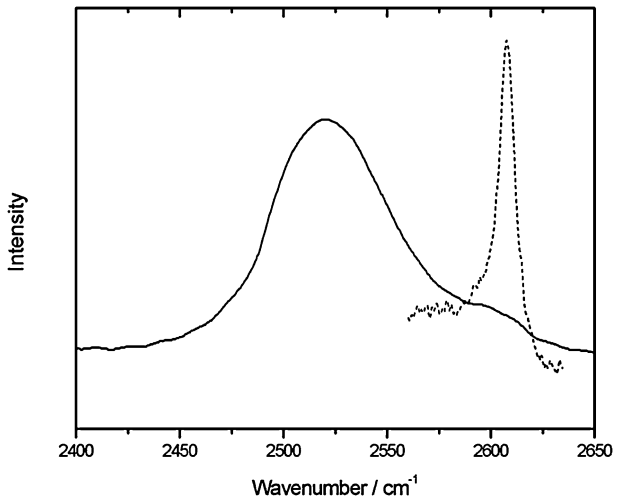

Fig. 1 FTIR spectra of DCN in d_8-THF (–) and $CHCl_3$ (---) in the ν_3 mode region. The two spectra have been arbitrarily vertically scaled. The DCN was produced photochemically so the concentrations in the two solutions were not determined.

measure vibrational relaxation time constants for the ν_1 and ν_3 modes of HCN and DCN. These measurements were carried out as described previously,[4,8] using a $\sim$2 ps duration, 12 cm^{-1} bandwidth IR excitation pulse, and the $\sim$500 cm^{-1} bandwidth probe pulse at time delays from 0–250 ps.

3. *Ab initio* reaction energetics and development of an analytical Hamiltonian

To aid interpretation of the time-resolved IR absorption data, calculations were undertaken of the dynamics of reaction (1) in neat THF. There were two components to this work: first, we used electronic structure theory and some recently developed dynamics codes to derive an accurate potential energy surface (PES) representation of an abstraction pathway for the reaction, and second we used the PES to run batches of molecular dynamics reactive simulations. All electronic structure theory calculations in this work were carried out using the MOLPRO suite of programs.[23]

THF may undergo hydrogen abstraction at either the 2 or 3 position, respectively yielding a 2-tetrahydrofuranyl radical (2-C_4H_7O) or a 3-tetrahydrofuranyl radical (3-C_4H_7O). In our previous work,[4–6] we examined similar secondary hydrogen abstraction reactions for CN + propane and CN + cyclohexane. Our study showed that non zero-point corrected reaction energies at the restricted open-shell ROMP2/aug-cc-pVDZ level of theory agreed to within 1 kcal mol^{-1} with higher level UCCSD(T)-ROHF calculations extrapolated to the infinite basis limit. Accordingly, the energies for reaction (1) reported in Table 1 were obtained at the ROMP2/aug-cc-pVDZ level of theory, which is significantly more computationally efficient than UCCSD(T)-ROHF calculations. The reaction energies in Table 1 are in good agreement with the experimental CN + C_3H_8 298 K reaction enthalpy of −29 kcal mol^{-1}.[24–26] As is shown in Table 1, abstraction of an H-atom from the 3 position is less exothermic than abstraction from the 2 position.

Table 1 Classical reaction energies for reaction (1) yielding both 2-tetrahydrofuranyl and 3-tetrahydrofuranyl radicals

Reaction	ROMP2/aug-cc-pVDZ
CN + C_4H_8O → HCN + 2-C_4H_7O	−31.0 kcal mol^{-1}
CN + C_4H_8O → HCN + 3-C_4H_7O	−26.1 kcal mol^{-1}

In the molecular dynamics described later, we investigated the less exothermic of the two abstraction reactions (*i.e.*, CN + C_4H_8O → HCN + 3-C_4H_7O), since that process should represent an approximate lower limit to the amount of vibrational excitation which may be localized in the nascent HCN. Running a large number of solution phase trajectories using direct dynamics calculations employing the electronic structure methods discussed above is computationally expensive, and furthermore, while the ROMP2 energies in Table 1 are adequate for the purposes of calculating the reaction energy, they provide a less satisfactory representation of the energy profile along the abstraction reaction coordinate. Consequently, our strategy has been to compute CCSD(T)/aug-cc-pVDZ energies along the reaction coordinate with ROMP2/aug-cc-pVDZ geometries obtained from a relaxed scan along this coordinate. In the atomic numbering scheme that we used for reaction (1), hydrogen atoms H10 and H11 are attached to the 3-Carbon in THF. Fig. 2 shows CCSD(T)/aug-cc-pVDZ//ROMP2/aug-cc-pVDZ energies along a reaction coordinate modelled as the distance between H11 and the C-atom in the CN radical. The barrierless energy profiles shown in Fig. 2 are very similar to the analogous multireference results of Klippenstein and co-workers for the CN + ethane reaction,[27] and our own results for CN + *c*-C_6H_{12},[5] with a preferred linear approach of the CN to the hydrogen atom, both in terms of the relevant C–H–C and H–C–N angles.

The computed energy profile shown in Fig. 2 was fitted using an analytical form of the PES. Our approach was to construct a reactive abstraction PES from a matrix representation of coupled, non-reactive molecular mechanics force-fields, $V(\mathbf{q})$. This method exploits the fact that molecular mechanics force-fields are generally well-calibrated for simulations of non-reactive dynamics, and has been described in our previous work.[5,6] Specific details for the CN + THF reaction are provided in the electronic supplementary information.

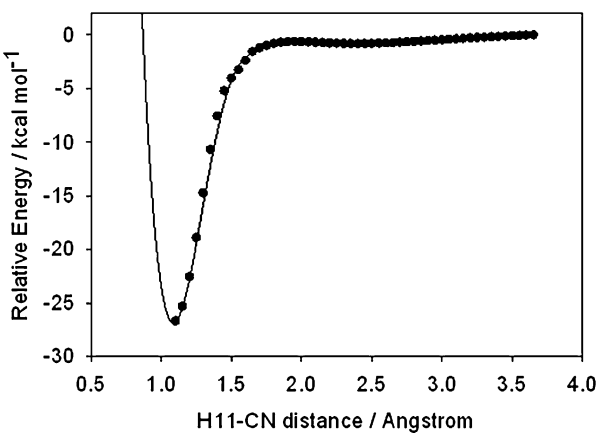

Fig. 2 Relaxed energy scans along the H11-CN distance for reaction (1) using (i) CCSD(T)/aVDZ//ROMP2/avdz electronic structure theory (●) , and (ii) the analytical PES (—) described in the text.

4. Results and discussion

UV pump and transient, broadband IR spectra were obtained for solutions of ICN in THF or d_8-THF, and for ICN/THF solutions in $CDCl_3$ or CD_2Cl_2. The latter experiments focussed on HCN formation so products of any reaction of CN radicals with the chlorinated solvent did not contribute to the observed IR spectra, except through formation of CN-solvent complexes,[13,14] as discussed further below. In this section, results are presented and analysed for reactions of CN radicals in neat d_8-THF and THF, giving DCN and HCN reaction products. These are followed by the outcomes of the experiments involving dilution of the ICN and THF reagents in $CDCl_3$ and CD_2Cl_2, after which comparisons are drawn between the computed reaction dynamics and the experimental observations. Interpretation of the results from the experimental bimolecular reaction studies requires knowledge of vibrational relaxation times of HCN and DCN in solution, and the determination of these time constants by transient IR-pump and IR-probe spectroscopy is therefore described first.

4.1 Time constants for vibrational relaxation of HCN and DCN in solutions containing THF

Transient IR absorption spectra for HCN excited by a ~2 ps duration IR pulse tuned into resonance with the 1_0^1 band at ~2070 cm^{-1} are shown in Fig. 3 (as differences between spectra with the IR pump laser on and off) for time delays between the pump and probe pulses from 0–25 ps. The spectra shown are for HCN dissolved in a 3.0 M THF/CD_2Cl_2 mixture, and the transient absorption on the 1_1^2 band centred at 2062 cm^{-1} is accompanied by a negative-going bleach in the 1_0^1 band associated with pumping of ground state molecules to $v = 1$ of the v_1 mode by the first IR pulse. The two bands are observed at different central wavenumber because of anharmonic shifts consistent with the known gas-phase spectroscopy of HCN.[28] The transient absorption on the 1_1^2 hot band decays through interaction with the solvent bath on the same timescale as the recovery of the ground state population (and hence loss of the bleach signal in the 1_0^1 band). Similar data are also presented in the figure for transient absorption on the 3_1^2 band and the bleach of the 3_0^1 fundamental band. Time-dependent integrated band intensities for transient absorption data such as those shown in Fig. 3 were fitted to exponential decays to determine relaxation time constants and the results are collected in Table 2 for HCN in THF, HCN in 3.0 M solutions of THF in $CDCl_3$ and CD_2Cl_2, and DCN in d_8-THF.

4.2 DCN products of the reaction of CN radicals in neat d_8-THF

Transient IR absorption spectra obtained for photolysis of ICN (0.14 M) in neat d_8-THF are shown in Fig. 4 in the wavenumber region 2375–2725 cm^{-1} corresponding to the v_3(C−D) stretch of DCN. Fig. 4(b) displays a broad feature centred at ~2520 cm^{-1} for times greater than 20 ps; on the basis of the spectrum in Fig. 1 and the observed time dependence shown in Fig. 4(c), we assign this to the v_3 (nominally C−D stretching) mode of DCN. A band centred at 1860 cm^{-1} also grows in with time, as shown in Fig. 4(d), and is assigned to the v_1 (C≡N stretching) mode of DCN, significantly shifted to lower wavenumber than for the gas phase (1925 cm^{-1}) or for

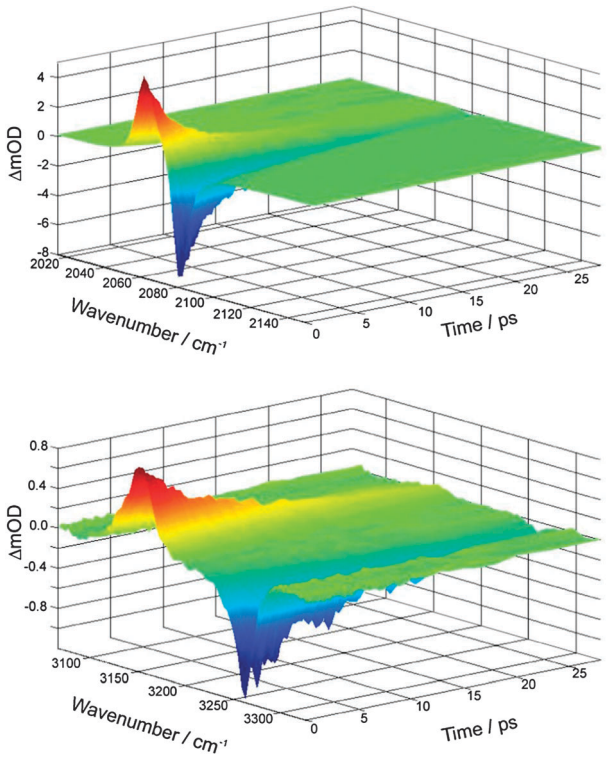

Fig. 3 Transient IR absorption spectra of HCN dissolved in a 3.0 M solution of THF in CD_2Cl_2 in the v_1 (C≡N stretching) region (top), and the v_3 (C−H stretching) region (bottom), following IR excitation of the fundamental band of each of these vibrational modes. Spectra are plotted as the difference in IR absorption with and without the IR pump laser. The positive signals are absorptions on vibrational hot bands, whereas the negative signals are transient bleaches of the fundamental bands.

solution in chlorinated solvents (~1919 cm^{-1}). In this region, the main feature is overlapped and distorted by a weak solvent absorption feature, so some caution must be exercised in interpretation of band shapes and time-dependences.

The transient IR spectra displayed in Fig. 4 are markedly different from those we reported for DCN formation from reaction of CN radicals with d_{12}-cyclohexane in solution in $CHCl_3$.[8] The bands rise in intensity much more quickly in d_8-THF and individual bands appear broader, but the spectra do not exhibit the previously observed multiple band structure. Both C−D and C≡N bands show a short induction period of 3–5 ps before the growth in intensity, and there is a clear shift of intensity from lower (~2465 cm^{-1}) to higher (centred at 2520 cm^{-1}) wavenumber with time in the band shown in Fig. 4(a). After ~50 ps, there is no further growth in intensity of either the C−D or C≡N stretching fundamental bands, and neither exhibits any decay in intensity on timescales as long as 2.5 ns, consistent with stable reaction products.

The time-dependent band intensities were analysed by first fitting the spectra to Gaussian functions to provide integrated absorption intensities. For the data in Fig. 4, two Gaussian functions were used with centres constrained to 2465 cm^{-1} and 2520 cm^{-1} (which is approximately consistent with the anharmonic shift of −41 cm^{-1} in the 3_1^2 hot band from the 3_0^1 fundamental

Table 2 Time constants for vibrational relaxation of HCN and DCN in various solutions containing THF (and ~0.14 M ICN, which was used to prepare the HCN by UV photolysis) as determined by transient IR absorption spectroscopy following IR excitation

	ν_1 (C≡N stretch)		ν_3 (C–H or C–D stretch)	
Solution	IR Pump	τ/ps	IR pump	τ/ps
HCN/THF	1_0^1 at 2080 cm^{-1}	4.7 ± 1.0		
HCN/3.0 M THF/$CDCl_3$	1_0^1 at 2080 cm^{-1}	3.2 ± 0.4	3_0^1 at 3260 cm^{-1}	7.0 ± 0.5
HCN/3.0 M THF/CD_2Cl_2	1_0^1 at 2080 cm^{-1}	3.1 ± 0.2	3_0^1 at 3260 cm^{-1}	7.4 ± 0.8
DCN/d_8-THF			3_0^1 at 2550 cm^{-1}	3.7 ± 0.1

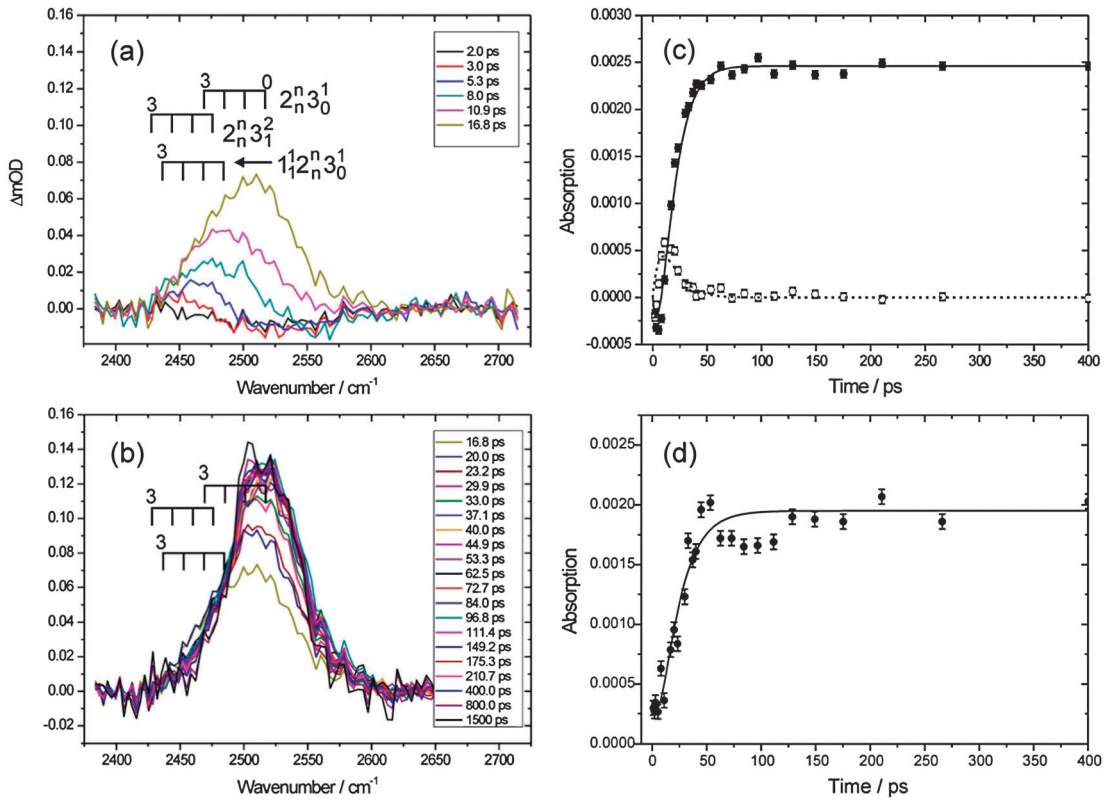

Fig. 4 Panels (a) and (b) show time-resolved IR spectra of DCN from reaction of CN radicals with d_8-THF in the ν_3 (C–D stretching) region at short (2.0–16.8 ps) and longer (16.8–1500 ps) time intervals. Combs show expected positions of various combination bands of the three modes of DCN (based on application of a constant solvent shift to gas-phase band origins). Diagonal progressions in the bend are indicated by 2_n^n with n = 0–3. Panel (c) shows the time dependences of integrated intensities of two features centred at 2465 cm^{-1} (open symbols and dashed line) and 2520 cm^{-1} (filled symbols and solid line). See text for details of the fitting procedures. For comparison, panel (d) shows the time dependence of the integrated intensities of a band centered at 1860 cm^{-1} (not shown) which is assigned to the ν_1 (C≡N stretch) fundamental.

of gas-phase DCN[22]) and with fixed and equal widths. For spectra obtained in the ν_1 region, which exhibit poorer signal to noise levels, there was no clear evidence of variation of the time-dependence with wavenumber across the band. Hence, a fit to a single Gaussian function located near the band centre was used to derive band intensities. Fig. 4(c) and (d) show the resultant time-dependences of integrated band intensities for these two spectral regions.

The transient feature identified in Fig. 4(a) and centred at 2465 cm^{-1} grows to a maximum within 10 ps, and decays on a timescale that is commensurate with the fast rise of the feature centred at 2520 cm^{-1}. This kinetic behaviour is indicative of formation of an intermediate species that relaxes to a stable product. An interpretation that is consistent with our prior observations for CN reactions with d_{12}-cyclohexane in $CHCl_3$,[8] the wavenumbers of the bands, and the magnitudes of the time-constants for vibrational relaxation reported in Section 4.1, is initial formation of vibrationally excited DCN molecules. Note that the timescale for relaxation to the vibrational ground state, DCN(000) must be significantly faster in d_8-THF than for d_{12}-cyclohexane in $CHCl_3$, where the time constant for exponential DCN(000) growth is ~150 ps. An alternative hypothesis is that the shift in the absorption wavenumber reflects a change of environment of the nascent DCN from close proximity to the d_7-THF radical co-product to an orientation in which the new C–D bond interacts most favourably with the solvent. This behaviour might be expected to cause a shift in band position from higher to lower wavenumber with time, however, and the balance of evidence favours the former interpretation—see later. We propose a

kinetic model for analysis of the time-dependent band intensities (with R denoting a c-C_4D_7O radical):

$$CN + D{-}R \rightarrow DCN^* + R \quad (3a)$$

$$CN + D{-}R \rightarrow DCN + R \quad (3b)$$

$$DCN^* \rightarrow DCN \quad (3c)$$

Here, DCN denotes a ground state, solvated product, DCN* indicates a short-lived intermediate (either vibrationally excited or incompletely solvated), and the third step in the scheme is relaxation of this intermediate through solvent interactions. We assign pseudo-first order rate coefficients k_a, k_b and k_c to these three processes because the d_8-THF is in excess, and fit the data either with an analytical solution to the rate equations, or using numerical integration, with the latter preferred because of potential singularities in the functional form for the analytical solution. The fitting model allows for the fact that transition dipole moments may differ for DCN and DCN*, and can incorporate the population differences between vibrational levels connected by an IR transition in determination of band intensities. This model neglects possible geminate recombination of CN radicals with I atoms, to form either ICN or INC, which might affect the derived rates of (3a) and (3b) because it represents a further loss process for CN radicals. INC formation is observed in our experiments (see later), but this is considered a minor channel because the transition dipole moment for the N–C stretching mode is very large compared to the C–N mode in ICN,[29] and we typically do not observe recovery of the bleach in the ICN following UV photodissociation.[4,8] Further (retrospective) justification for the neglect of the effects of geminate recombination comes from the values of the bimolecular rate coefficients for reactions (1) and (2) reported later.

The outcomes of the fits are shown in Fig. 4 and the resultant rate coefficients are $k_a = 0.047 \pm 0.015$ ps^{-1}, $k_b = 0.021 \pm 0.013$ ps^{-1} and $k_c = 0.137 \pm 0.035$ ps^{-1} (for averages of fits to 5 data sets, with uncertainties of 1 standard deviation, and the ratio of transition dipole moments for DCN and DCN* constrained to a value of unity[4]). The time-constant for step (3c) of 7.3 ± 1.9 ps is in reasonable agreement with that for vibrational relaxation of DCN(001) prepared by IR-excitation in d_8-THF solution, as shown in Table 2. Differences may stem from the nature of the microscopic solvation environment. The total (pseudo 1st order) rate coefficient for DCN formation is $k_{tot} = k_a + k_b$ and, using a density of d_8-THF of 0.985 g mL^{-1} (and thus a concentration of 12.3 M) this translates into a bimolecular rate coefficient for the reaction of $k_r = (5.5 \pm 1.6) \times 10^9$ M^{-1} s^{-1}.

In the spectral data and the fits, there are indications of negative signals at early time for the DCN(000). Although these negative values may derive from background subtraction errors, similar behaviour was observed in our prior studies of CN + cyclohexane reactions, and interpreted as a consequence of substantial population of the vibrationally excited levels at early times giving rise to a population inversion with the ground state.[4] The fits can only account for the induction periods of negative or zero signals before growth of DCN(000) absorption features if some account is taken in the model of the population difference between the ground and vibrationally excited levels. Here and later, we assume that the known rotational excitation of CN from ICN photolysis in the UV is either damped prior to reaction,[30] or does not affect the reactivity of CN towards d_8-THF and THF. From the arguments presented above, we infer that the transient species is indeed vibrationally excited DCN. The combs in Fig. 7(a), and past experience,[4] suggest C–D stretch and bending excitation, but C≡N stretching cannot be discounted. Transient IR spectra of the absorption in the ν_1 region do not show clear signal in the region where C–D stretch excited DCN would absorb, but interference from a solvent feature may mask any weak bands, and the signal-to-noise ratios in the spectra are poor in this region.

The fits return values of k_a that are greater than k_b by a factor of 2 or more, and therefore indicate a preference for formation of DCN *via* the intermediate, vibrationally excited DCN*. Indeed, by taking the ratio $k_a/(k_a + k_b)$ we estimate (70 ± 30)% of the DCN forms vibrationally hot. The rapid rise of signal in the C–D stretching spectral region is echoed in the data for the C≡N stretching region (Fig. 4(d)): a fit to the kinetic scheme including reactions (3a)–(3c) with k_c constrained to a value of 0.137 ps^{-1} gives $k_a = 0.053 \pm 0.014$ ps^{-1}, in good agreement with the value for this rate coefficient derived from fits to the C–D stretching region spectra. This behaviour is expected if the absorption bands of the vibrationally excited molecules are shifted by anharmonicity to lower wavenumbers than are incorporated in our fits to the 1_0^1 band profiles.

4.3 HCN products of the reaction of CN radicals in neat THF

Observations of HCN products of reaction of CN radicals with undiluted THF were restricted to the C≡N stretching region at wavenumbers around 2070 cm^{-1} because of strong interference from THF bands in the region of absorption features associated with the C–H stretching vibrational mode. Representative transient IR absorption spectra for the ICN/THF solutions are shown in Fig. 5 for different time delays between the UV photolysis and IR probe laser pulses. Bleach of the ICN absorption band by the photolysis laser is not shown in the figure, but is observed as a negative signal at ~2160 cm^{-1} in such experiments that shows no recovery, indicating recombination to ICN is a minor channel for CN loss. The two features evident in the spectra are assigned to the 1_0^1 fundamental C≡N stretching band of HCN (2073 cm^{-1}) and an N–C stretching fundamental vibration of the INC molecule (2052 cm^{-1}). In the gas phase, the wavenumber of the ν_1 mode of HCN is 2097 cm^{-1},[28] so there is a modest (−24 cm^{-1}) solvent shift to lower wavenumber in THF solution that is less than the −65 cm^{-1} shift of the equivalent band for DCN in d_8-THF (perhaps because the ν_1 mode in DCN involves some C–D vibrational motion, and the C–D moiety can interact with the O-atom in THF). The band at 2052 cm^{-1} is assigned to INC on the basis of reports that this molecule absorbs in the range 2053–2063 cm^{-1} in Ar, Kr, Xe and N_2 matrices.[31] Both HCN and INC features were also observed in our studies of CN radical reactions in chlorinated solvents,[4] but a further band that was seen at 2037 cm^{-1} is absent in the experiments conducted in THF. Because of the match

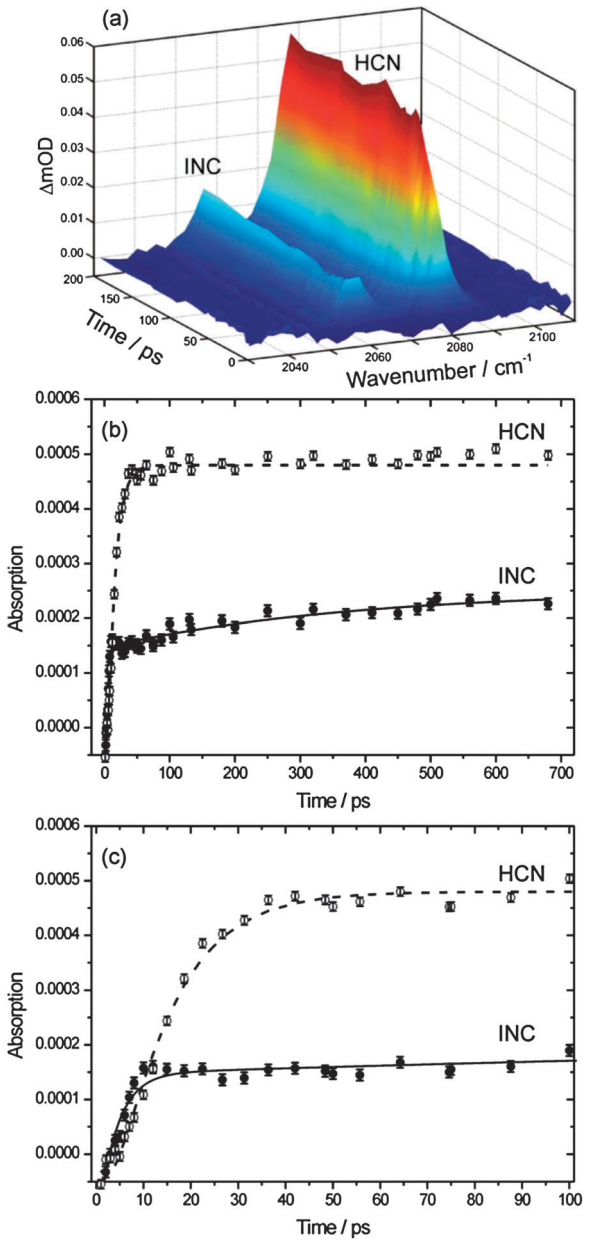

Fig. 5 (a) transient IR spectra from reaction of CN radicals with THF, obtained in the C≡N stretching region of HCN. The bands centred at 2052 and 2073 cm^{-1} are, respectively, assigned to INC and HCN(000). (b) time-dependence of integrated band intensities for the INC (●) and HCN (○) bands, with fits described in the text. (c) as for panel (b), but showing the early time data on an expanded scale.

to the wavenumber of the fundamental vibrational transition of gas-phase CN radicals, the carrier of this band was argued to be CN weakly complexed to a solvent molecule.[4,13,14] The absence of such a feature in the THF solutions suggests either that there is no CN complexation to THF, or that the CN is consumed more rapidly and completely by reaction.

The spectral bands were fitted to Gaussian functions with fixed centres at wavenumbers of 2073 and 2052 cm^{-1}, and representative time dependences of the integrated areas of the fitted functions are plotted in Fig. 5(b) and (c). The INC band exhibits two regions of different time dependence, a very rapid rise for the first ~10 ps followed by a steady increase over several hundred picoseconds. A fit to a bi-exponential function gives respective time constants of (4.0 ± 0.7) ps and (350 ± 190) ps (averages from three independent measurements). The fitted amplitude of the long-time contribution to the signal is ~1/3 that of the faster rising INC component. This behaviour suggests fast recombination of I and CN within a solvent cage accounting for ~75% of the product INC, with slower diffusive recombination after escape from the initial solvent shell contributing the remaining 25%. The rapid initial rise in intensity of the INC band in THF was also observed in reactions of CN studied in solution in $CDCl_3$, $CHCl_3$ and CH_2Cl_2, but constituted a lower fraction of the total INC yield: for example, for INC production in a 1.5 M cyclohexane solution in $CDCl_3$, only ~26% forms with a time constant of (21 ± 8) ps attributed to in-cage recombination, and the remaining 74% grows with a time constant of (520 ± 210) ps. The differences in the in-cage recombination fractions and time constants may reflect the propensity for CN to form complexes with the chlorinated organic molecules,[13,14] but to a lesser extent with THF, or may indicate a greater ease of escape of photolytically produced CN from the initial solvent cage in the case of the chlorinated solvents.

The HCN signal from reaction of CN with THF shows a fast rise following an initial induction of ~5 ps, reaching an almost constant absorbance after ~30 ps. In our prior studies of CN reactions in solutions of cyclohexane in chlorinated solvents, absorption *via* the 3_0^1 C–H stretching fundamental band appeared after a time delay of 50–100 ps.[4] At earlier times, the spectra instead exhibited zero or weakly negative signal because of the significant population of the $v_3 = 1$ vibrational level. The 3_1^2 vibrational hot band, and combinations of this band with hot-bands in the bending vibration, rose on much faster timescales, reaching maximum intensity within ~50 ps before decaying through vibrational relaxation to the ground state. In the current experiments in THF, with observations restricted to the C≡N stretching region, signatures of nascent HCN formed with C–H stretch and bending excitation above the zero-point level would be a shoulder on the low wavenumber side of the 1_0^1 band (corresponding to $1_0^1 2_n^n 3_1^1$ combination/hot bands), extending towards and overlapping the INC feature, and some delay to the rise of intensity at the centre of the 1_0^1 band. This latter delay will be governed by the vibrational relaxation rate of HCN in THF. The former effect is not clearly observed because of spectral congestion and signal-to-noise levels, although there is a small overshoot of the experimental data assigned to INC from the bi-exponential fit evident in Fig. 5(c) at times of ~7–15 ps that would correspond well with transient formation of vibrationally hot HCN (compare the transient feature in Fig. 4(c)). The observed ~5 ps induction time of the HCN(000) signal is consistent with much of the nascent HCN being vibrationally excited, and relaxing on the <8 ps timescale measured by IR-pump and IR-probe experiments and reported in Table 2. Again, we emphasize that this relaxation of vibrationally excited HCN is significantly faster than in the chlorinated solvents used in our previous studies.[4,8]

The HCN data were fitted to a kinetic scheme equivalent to eqn (3a)–(3c), but with H replacing D and R = *c*-C_4H_7O.

Fits to 3 data sets gave $k_a = 0.127 \pm 0.028$ ps^{-1}, $k_b = 0.063 \pm 0.016$ ps^{-1} and $k_c = 0.109 \pm 0.002$ ps^{-1}. The latter value corresponds to a vibrational relaxation time constant of $\tau = 9.2 \pm 0.2$ ps that is similar to those reported in Table 2. From the sum of k_a and k_b, and the density of THF (0.889 g^{-1} mL^{-1}), a bimolecular reaction rate constant $k_r = (1.54 \pm 0.36) \times 10^{10}$ M^{-1} s^{-1} is derived, and this value is discussed further in section 4.4. The branching to vibrationally excited HCN is estimated to be (67 ± 19) %. The almost flat HCN signal levels for times longer than 30–40 ps indicate only a minor contribution ($\leq$5%) from delayed or diffusive reactivity of the CN with the solvent.

4.4 HCN products of the reaction of CN radicals with THF diluted in $CDCl_3$ or CD_2Cl_2

To examine further the contrasting roles of THF and chlorinated solvents (as examined in prior work on CN + cyclohexane reactions[4,8]) on the condensed phase dynamics of CN radical reactions, measurements were made of transient IR spectra of HCN following UV photodissociation of 0.14 M solutions of ICN in THF/$CDCl_3$ or THF/CD_2Cl_2 liquid mixtures. In these experiments, the THF concentration was varied in the range 0.5–8.2 M, with neat THF corresponding to 12.3 M.

As Fig. 6 shows, in the ν_1 C≡N stretching region of HCN we see three bands that resemble those we observed previously for CN + cyclohexane reactions in chlorinated solvents,[4] and that we assign to a CN-solvent complex, INC and HCN(000). When CD_2Cl_2 is used as a solvent, it contributes a weak band that partially overlaps the HCN(000) feature. Fits to 3 Gaussian functions give the time-dependence of the integrated band intensities shown in the figure (neglect of the fit to the weak CN-solvent feature makes little difference to the analysis). The HCN bands show no significant shift of line centres as the solution composition is changed from 0.8–4.5 M THF, but the ratios of HCN to INC and CN-solvent complexes increase with increasing THF fraction, whereas the INC to CN-solvent complex ratio remains fairly constant. The timescale for rise of the 1_0^1 band of HCN(000) is considerably faster than we reported for the CN + cyclohexane reactions in similar solvents.

The change in appearance of the spectra with THF concentration is striking, and is largely a consequence of the increasing INC signal and its shift to higher wavenumber as the THF fraction decreases. The HCN 1_0^1 band is centred at 2079 cm^{-1} in the THF/$CDCl_3$ solutions (and 2073 cm^{-1} in neat THF), compared to 2094 cm^{-1} in cyclohexane/chloroform solutions, giving greater overlap with the INC band than in our previous experiments.[4,8]

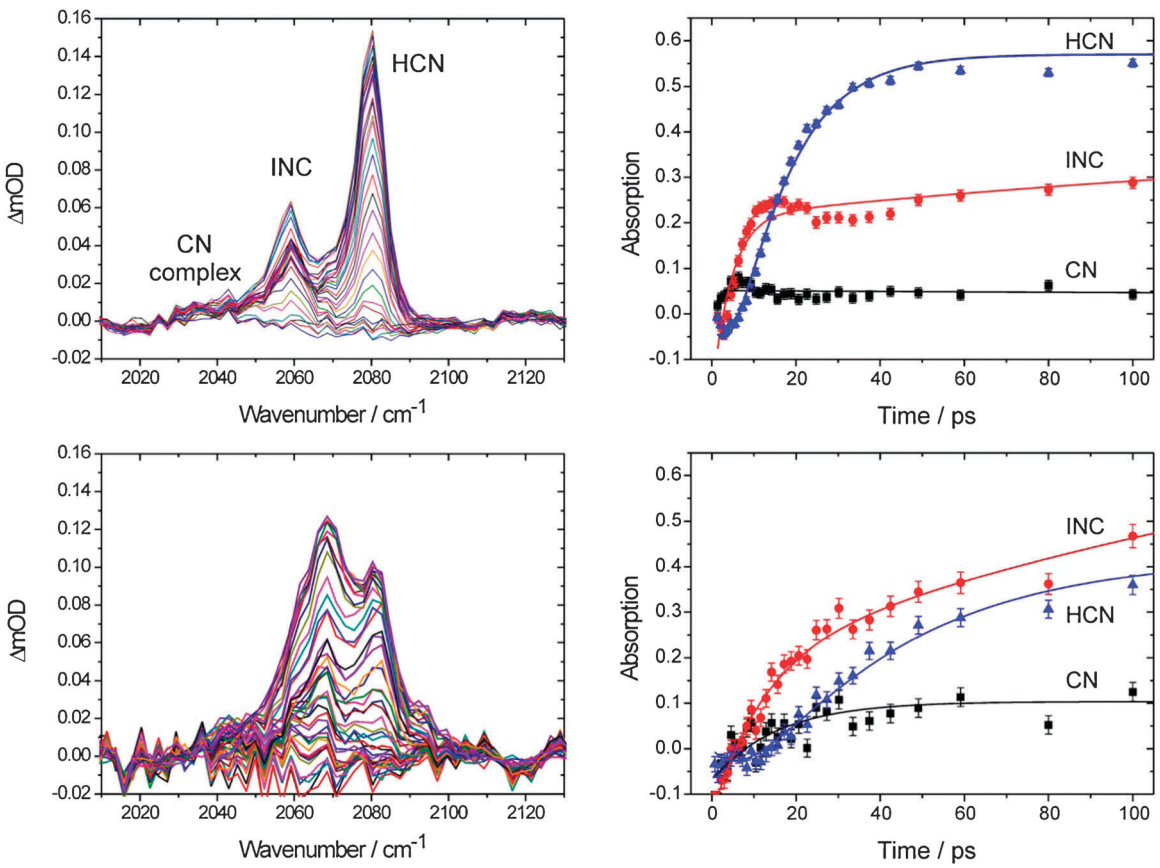

Fig. 6 The left-hand column shows time-resolved IR spectra for formation of HCN (in the ν_1 C≡N stretching region, with band centre at 2079 cm^{-1}) and INC in solution in THF and $CDCl_3$ with THF at a concentration of 8.2 M (top) and 2.0 M (bottom). The weak feature to the low wavenumber side of the INC band is assigned to CN-solvent complexes. The spectra are shown over time intervals from 0–2000 ps and all features grow with time. The time dependences (first 100 ps) of integrated absorptions of features assigned to HCN (blue triangles), INC (red circles) and CN complex (black squares) for both solutions are shown in the right hand column. Solid lines are fits to the data that are discussed in the text.

Table 3 Estimated fraction of INC formed by in-cage recombination in THF/$CDCl_3$ solutions of various THF concentrations

THF concentration/mol dm^{-3}	0.0	2.0	4.1	8.2	12.3
In-cage fraction of INC	0.25	0.42	0.59	0.67	0.75

The data displayed in Fig. 6 are for dilution in $CDCl_3$, and similar data were obtained for CD_2Cl_2. In the latter solvent, the INC band appeared sharper and the CN-solvent complex band was more evident. This CN-solvent feature exhibits a rise time of ~4 ps in CD_2Cl_2. The plots in Fig. 6 indicate both a prompt and a long-time diffusive rise of INC, the latter having a time constant of ~200 ps regardless of solvent and THF fraction. Comparison of the amplitudes of the fast and slow contributions to the INC signals can be used to estimate the degree of in-cage *versus* diffusive recombination as the fraction of THF in the solvent increases, and these estimates are shown in Table 3. The rate coefficients for the fast component of the rise of INC for ICN/THF/$CDCl_3$ and ICN/THF/CD_2Cl_2 are plotted in Fig. 7 and increase with increasing THF fraction, but show no clear dependence on the choice of chlorinated solvent. The similarity of their dependence on the concentration of THF with that for the bimolecular reaction rate coefficients (see later) suggests that the removal of CN radicals by reaction is what controls the observed recombination rate to form INC (consistent with this recombination being a minor channel for CN loss).

Careful inspection of the INC data in Fig. 6 for 8.2 M THF shows a small peak in the IR absorption intensity in the vicinity of the INC signal at time delays of 7–20 ps, much as was remarked upon for neat THF in section 4.3. This additional absorption may be a signature of vibrationally excited HCN, for which the absorption bands are shifted to lower wavenumber than the 1_0^1 fundamental band.

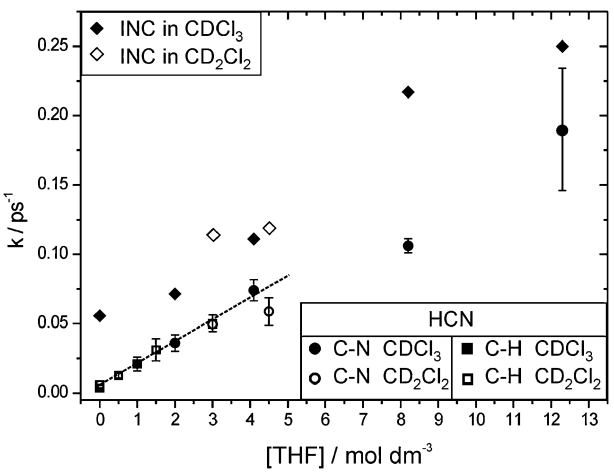

Fig. 7 Rate coefficients for the rise in absorption band intensities for HCN (circles and squares) and INC (diamonds) in solutions of THF in $CDCl_3$ (filled symbols) and CD_2Cl_2 (open symbols). For HCN, data are shown for both the C−H (squares) and C≡N (circles) spectral regions. The dependence of the rate coefficients on THF concentration is shown, with 12.3 M corresponding to neat THF. The dotted line highlights the linear dependence of the pseudo-first order rate coefficient for HCN production on THF concentration up to 4.5 M, and this dependence would appear to continue as far as neat THF (although with larger uncertainties).

Fig. 7 also compares the rate coefficients for total HCN formation in the various ICN/THF/$CDCl_3$ and ICN/THF/CD_2Cl_2 solutions of differing THF concentrations from fitting of the intensities of the HCN 1_0^1 band at 2079 cm^{-1}, examples of which are shown in Fig. 6. In general, k_a was found to be much greater than k_b in trial fits to reactions (3a)–(3c) for various concentrations of THF (an observation that is in good agreement with our molecular dynamics simulations, as will be discussed in section 4.5), so k_b was constrained to zero and the total rate coefficient for HCN formation was therefore equated with k_a. The linear increase in rate coefficients with concentration of THF (up to 4.5 M, and perhaps beyond) is consistent with pseudo-first order kinetics with the THF in excess over CN radicals, and is discussed further below. As before, we assume in this analysis—with justifications as described previously—that the removal of CN by reaction dominates its loss by geminate recombination to INC and ICN under all conditions. A more complete analysis of the kinetics might incorporate Smoluchowski behaviour to allow for time-dependence of the bimolecular rate coefficients associated with changes in the local THF concentration,[11,12] but these more subtle effects are neglected in our current fitting.

Spectra obtained in the C−H stretching region show a band assigned to the fundamental 3_0^1 absorption by HCN(000) that is centred at ~3260 cm^{-1}, but the expected location of the HCN 3_1^2 hot band ~100 cm^{-1} to lower wavenumber, previously observed for CN + cyclohexane reactions in chlorinated solvents, is obscured by an overlapping THF band. Fig. 8 shows time-dependences of the 3_0^1 feature obtained by integrating the absorption bands using fitting to a single Gaussian function for two different concentrations of THF in CD_2Cl_2, and the rate coefficients resulting from fits of these time-dependent band intensities to a kinetic scheme equivalent to reactions (3a)–(3c) (with D replaced by H) are included in Fig. 7. As with the C≡N stretching region data, we found $k_a \gg k_b$, implying the dominant reaction pathway is to vibrationally excited HCN, and k_b was therefore constrained to zero in the kinetic fits. The pseudo-first order rate coefficients for HCN formation are thus the k_a values from the fits, and each point plotted in Fig. 7 is the average of fits to between 2 and 6 data sets, with error bars representing 1 standard deviation. The values obtained from analysis of C−H stretching bands are in quantitative agreement with those derived from spectra in the C≡N stretching region, and the choice of solvent (CD_2Cl_2 or $CDCl_3$) has no discernible effect.

The C−H stretching band intensities are much weaker than might be expected from comparison with C≡N stretching mode absorption features, and comparison of spectra for ICN/THF/CD_2Cl_2 and ICN/cyclohexane/CD_2Cl_2 samples with equivalent concentrations of THF and cyclohexane under otherwise identical conditions indicates ~5-fold greater signal levels for cyclohexane than for THF reactions. We attribute these observations to a partitioning of the HCN in the current experiments between environments where it is solvated by the chlorinated solvent or THF, with the latter being favoured. Hydrogen bonding of HCN to THF may cause a significant shift of the C−H vibrational frequency to lower wavenumbers that lie outside our spectral observation window.

The signals in Fig. 8 show an initial induction period of 5–15 ps, similar to the C≡N region data, followed by a rise in signal,

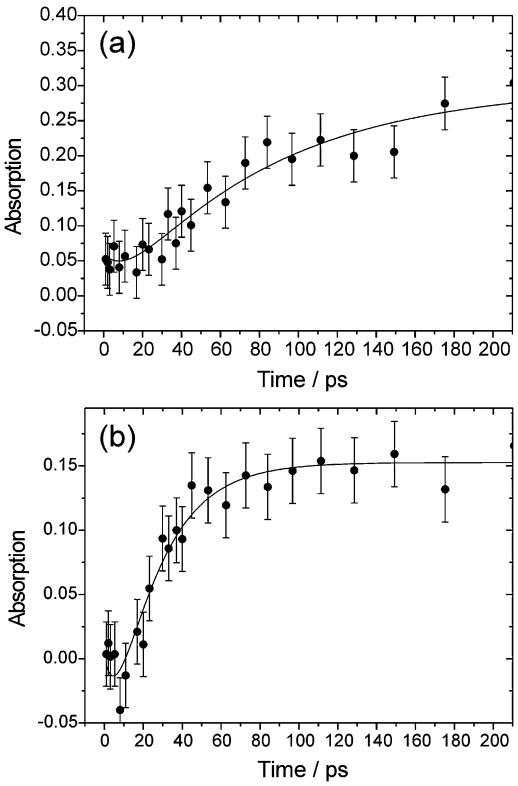

Fig. 8 Time dependence of band-integrated absorptions for the ν_3 C−H stretching fundamental of HCN formed by reaction of CN radicals with THF in CD_2Cl_2: (a) 0.5 M THF; (b) 3.0 M THF. Black circles are experimental measurements and solid lines are fits to the kinetic model described in the text. Data are shown for the first 200 ps, but were accumulated at time intervals up to 2500 ps and were fitted over this full range. The data showed no longer-time rises beyond the absorption levels plotted.

the rate of which increases as the THF fraction increases. For THF concentrations up to 4.5 M, the rate coefficients for the formation of HCN, as determined from the C−H stretching region IR absorption spectra, show the same linear dependence on THF concentration as those obtained from the spectra in the C≡N region (see Fig. 7). The agreement between C−H and C≡N region data confirms that the IR spectra are observing the same process. A weighted linear fit to the C−H and C≡N region pseudo first order rate coefficient data for THF concentrations up to 4.5 M gives a bimolecular rate coefficient $k = (1.57 \pm 0.12) \times 10^{10}$ M^{-1} s^{-1} that agrees well with the value obtained above for neat THF and that is very similar to the reported rate coefficient of $(1.4 - 1.8) \times 10^{10}$ M^{-1} s^{-1} for the CN + ethane reaction in the gas phase at 292 K,[32,33] providing further evidence that we are indeed determining the rate of the bimolecular reaction in solution.

If the growth in the 1_0^1 and the 3_0^1 band intensities both derive from the same vibrational relaxation of nascent HCN, time-dependent data obtained on both bands for the same concentrations of reagents and a particular solvent should fit simultaneously to the same kinetic model. For ICN (0.14 M)/THF (3.0 M)/CD_2Cl_2 solutions, spectral data obtained in the C≡N and C−H stretching regions can be compared directly, and the time-dependent band intensities (averaged over four measurements for the C≡N region and two for the C−H region) were analysed. A model was used in which, HCN(100), HCN(001) and HCN(000) were produced by the chemical reaction of CN with THF, and the vibrationally excited products underwent relaxation to HCN(000) in single-quantum steps. Simultaneous fits, which incorporated population differences in determining the band intensities from time-dependent HCN concentrations, converged to a solution in which the rate coefficient for HCN(001) was at least a factor of 5 larger than for reactions forming HCN(100) and HCN(000). C−H stretch excited HCN is therefore judged to be the main product of the reaction, consistent with a transition state that is early along the reaction coordinate,[5] and in keeping with our prior studies of reactions of CN with cyclohexane and tetramethylsilane in solution.[4,8] However, vibrational relaxation of the C−H stretch excited HCN is much more rapid than that for CN reactions with cyclohexane in chlorinated solvents.[4,8]

The data encourage an interpretation in which most of the HCN is formed with C−H stretching vibrational excitation (in qualitative agreement with the molecular dynamics results discussed in section 4.5), despite the presence of the solvent. However, the nascent products relax very quickly to the vibrational ground state by coupling to the solvent bath. Spectral overlap of the HCN 3_0^1 band with a THF band suggests the possibility of resonant vibrational energy transfer from HCN to THF (or to the radical co-product[6]) that may promote the relaxation step, whereas the two chlorinated solvents $CDCl_3$ and CD_2Cl_2 appear to play essentially identical and more weakly interacting roles. The weaker absorption in the C−H region for the THF experiments prevents the type of detailed analysis of the bending excitation of the HCN or DCN products that we carried out for cyclohexane reactions.[4,8]

4.5 Computational molecular dynamics of the CN + THF reaction

4.5.1 Methods. The molecular dynamics simulations discussed below provide support for the conclusion that CN reaction with THF produces very little nascent HCN(000), with the majority being vibrationally excited and with the energy mostly located in the C−H stretch. Using the CHARMM software suite[34] with the Hamiltonian discussed in section 3 and electronic supplementary material, we carried out 200 solution phase dynamics trajectories. Each involved two different runs: a leap-frog Verlet NVT equilibration run followed by an NVE trajectory. NVT equilibration runs lasted 200 ps (0.5 fs timestep), with a Langevin friction coefficient of 10 ps^{-1}. The subsequent NVE trajectories had durations of 100 ps and used 0.1 fs time-steps. CN and THF were solvated within a 23.8 $Å^3$ periodic box filled with 100 molecules of THF, corresponding to the 298 K THF density of 0.889 g mL^{-1}.

On the timescale of the simulations, every single CN + THF trajectory was reactive and resulted in the HCN + 3-C_4H_7O radical. The probability of obtaining reactive events was accelerated using the AXD (Accelerated Molecular Dynamics) algorithm,[35] which is a formally exact extension of TST that accelerates reactive events by implementing phase space constraints in a fashion that conserves angular momentum, linear momentum, and energy. As such, it works equally well for

both NVT and NVE simulations. It does not perturb chemical dynamics in the neighbourhood of a TS so long as the distance between the phase space constraint and the TS is larger than the system's characteristic decorrelation length.[36] In the NVT simulations, we implemented a phase space constraint that maintained the H11–CN distance to be between 2.5 and 4.0 Å, which corresponds to the reactant side of the abstraction TS. In the NVE simulations, the 2.5 Å constraint was relaxed, allowing barrier crossing and subsequent abstraction to proceed with significant acceleration, essentially by preventing diffusion of the reactants away from one another.

To obtain the potential of mean force (PMF) along the H11-CN coordinate, we used the BXD (Boxed Molecular Dynamics) algorithm[35] in conjunction with the respective NVT simulation details described above. BXD is a multiple-constraint extension of AXD, which can be used to obtain accurate potentials of mean force and rate coefficients. In the BXD simulations carried out as part of this work, we used 6 simulation boxes, with configuration space velocity inversion boundaries at 1.25, 1.35, 1.5, 1.6, 1.7, 2.0, 4.0, and 6.0 Å. Convergence of the PMFs was monitored on each pass through the boxed configuration space. Both the AXD and BXD algorithms have recently been implemented in CHARMM.

For those reactive trajectories which yielded HCN using the methods described above, mode dependent energy content of the nascent HCN was determined by projecting its space-fixed Cartesian velocities, $\dot{\mathbf{q}}(t)$, and coordinates, $\mathbf{q}(t)$, into the translational, rotational, and vibrational normal modes of HCN in its centre-of-mass (CM) frame equilibrium geometry, $\mathbf{q}_{eq}$. In order to carry out this analysis, the nascent HCN was translated to its CM frame, and the least squares difference between the mass-weighted coordinates of the nascent HCN and those of the equilibrium HCN was minimized with respect to rigid-body rotations using singular value decomposition—an operation which is identical to placing the rovibrationally hot HCN into the Eckart frame of the equilibrium HCN, thereby minimizing rovibrational Coriolis coupling in the reference frame of the nascent HCN.[37–39] Then, we transformed the Cartesian coordinates and velocities into the translational, rotational, and vibrational displacements of the equilibrium geometry as described previously.[5] Table 4 shows a comparison between the experimental HCN rotational constants (expressed as moments of inertia) and vibrational frequencies[40] and those obtained using the MMFF.

Simulations were also carried out to probe the sensitivity of HCN relaxation timescales in solution in THF to the spectral overlap of solvent and solute molecules. Three sets of simulations were performed for HCN in a periodic box of 100 THF solvent molecules with decreasing values of the H-CN stretching force constant. For each set, 20 NVE trajectories were computed with each trajectory lasting 200 ps (with a 1 fs timestep) from initial conditions generated from NVT equilibration runs identical to those described above.

Table 4 Frequencies and moments of inertia of HCN obtained from experiment[40] and the MMFF force-field

	Moments of Inertia/amu Å^{-2}	Vibrational Frequencies/cm^{-1}
Experiment	11.404	3311, 2097, 712 (×2)
MMFF	11.516	3470, 2019, 777 (×2)

4.5.2 Results. Fig. 9 shows the relative 298 K PMF for reaction (1) in a solvated box of THF, plotted along the H11–CN abstraction coordinate (to form HCN + 3-C_4H_7O), and obtained using the BXD method. Despite the fact that the reaction is barrierless on the PES, Fig. 9 shows a maximum at a separation of ~1.8 Å. The origin of this maximum is primarily entropic, corresponding to a reduction in relative fragment rotational and translational degrees of freedom as CN approaches THF to abstract hydrogen H11.

The outcomes of the trajectory calculations are shown in Fig. 10 as normalized distributions of the energy (above the zero-point energy of HCN) deposited in the various HCN degrees of freedom a few picoseconds after passage over the solution-phase variational TS shown in Fig. 9. The distributions are similar to those obtained in our previous experimental and theoretical work on the CN + c-C_6H_{12} reaction,[4–6] which

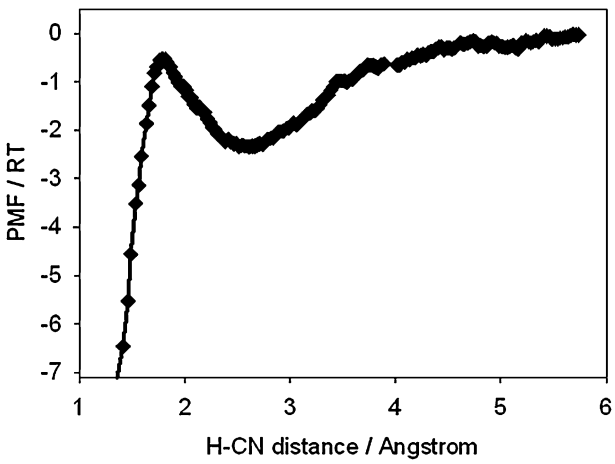

Fig. 9 Plot of the 298 K potential of mean force along the H11-CN distance for reaction (1) solvated in THF.

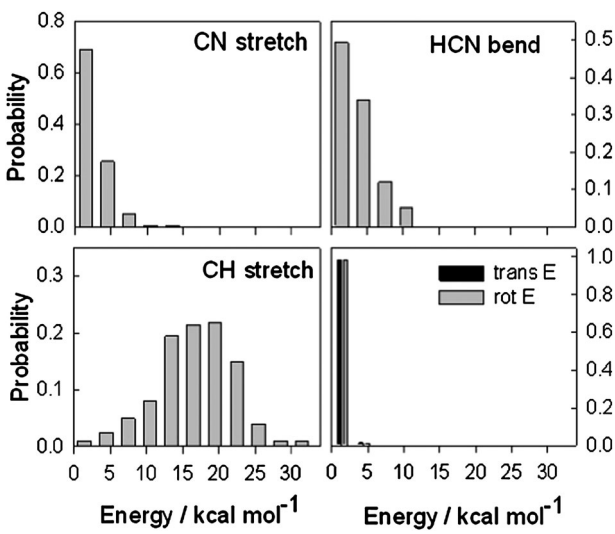

Fig. 10 Normalized distributions of energy deposited into each HCN degree of freedom for reaction (1) in a solvated box of THF. Results have been placed into bins with width of 3 kcal mol^{-1}.

showed vibrational excitation in the nascent HCN for both the v_3 (C−H stretch) and the v_2 (HCN bend) modes. For reaction (1), the C−H stretch energy distribution peaks around 19.5 kcal mol^{-1} with an average of ~17.5 kcal mol^{-1}. This average lies between 10.5 and 20.4 kcal mol^{-1} which are the expected energies for $v_3 = 1$ and $v_3 = 2$ excitation in the C−H stretch. Reaction (1) is ~5.4 kcal mol^{-1} more exothermic than the CN + c-C_6H_{12} reaction, and this extra available energy appears to promote greater C−H stretching excitation, with very little HCN formation in $v_3 = 0$. For reactions leading to HCN + 2-C_4H_7O, the nascent HCN(000) population is likely to be even smaller. The simulations suggest that the C≡N stretching mode of the HCN product does not contain significant vibrational excitation above the zero point level, in accord with experimental deductions.

The average time-dependent mode energies of HCN derived from trajectories are shown in Fig. 11, with the zero of time corresponding to the first passage through the C−H distance of HCN at equilibrium. Fig. 11 shows that the C−H stretching excitation seen in Fig. 10 dissipates into the solvent over time. In previously published work,[6] we used molecular dynamics methods to analyze HCN relaxation following H abstraction from c-C_6H_{12} in solution in CH_2Cl_2, and observed a distinct separation in C−H relaxation timescales, with faster relaxation occurring at short times when the nascent HCN was in close proximity to the c-C_6H_{11} co-product radical. Slower relaxation occurred following diffusion of the HCN away from its product partner c-C_6H_{11} into the bulk CH_2Cl_2 solvent. In light of these observations, we note that Fig. 11 does not show such a clear separation in C−H relaxation timescales. The reason for this is likely to be because the spectral properties of the nascent 3-C_4H_7O radical are similar to those of the bulk THF solvent, unlike the case of c-C_6H_{11} in bulk CH_2Cl_2. Hence, HCN does not experience as large a change in its chemical environment upon diffusing away from its radical co-product.

The fraction of nascent HCN with C−H energy greater than that corresponding to the $v_3 = 1$ stretching energy (10.5 kcal mol^{-1})

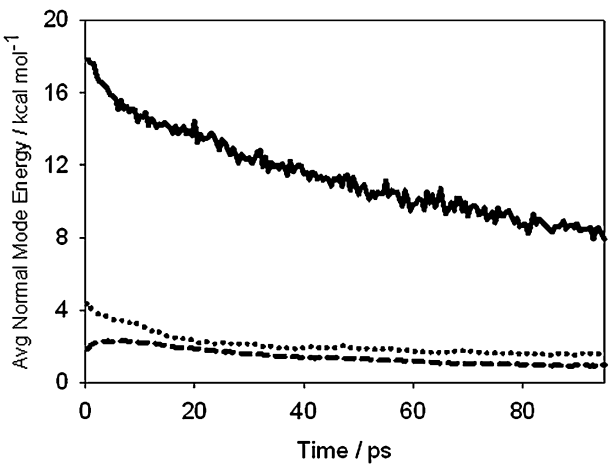

Fig. 11 Time-dependent vibrational mode energies in the nascent HCN following abstraction of a hydrogen atom from THF in the solution phase simulations: --- v_1 (C≡N stretch); ··· v_2 (bend); — v_3 (C−H stretch). Results shown are averaged over 200 reactive trajectories.

decays with time because of dissipation of this vibrational excitation to the solvent environment. To a good approximation, the decay of vibrationally excited HCN(00n) ($n \geq 1$) follows a bi-exponential decay:[41]

$$\mathrm{HCN}(00n)(t) = Ae^{-t/\tau_1} + Be^{-t/\tau_2} \quad (4)$$

where τ_1 and τ_2 are the associated decay time constants. Using eqn (4) to fit the C−H vibrational energy deactivation gives $\tau_1 = 11.2 \pm 3.2$ ps and $\tau_2 = 87 \pm 1.5$ ps, with $A = 0.089 \pm 0.026$ and $B = 0.928 \pm 0.007$. The faster time constant agrees well with the experimental deductions of fast vibrational relaxation of the nascent HCN. However, a decay corresponding to the second time constant was not resolved by the experiments (see, for example, Fig. 5). This apparent discrepancy may be a consequence of the signal-to-noise levels in the experiment being inadequate to resolve a long-time rise in HCN, or an underestimate by the calculations of the significance of the early-time coupling of HCN vibrational energy to the radical co-product and solvent bath (*i.e.*, the relative magnitudes of A and B in eqn (4)). It may also be that changes in the solvation environment of the HCN caused by diffusion and complexation to solvent molecules shift the wavenumbers of the HCN 1_0^1 and 3_0^1 bands out of our IR absorption observation window in the experimental measurements. However, such a shift might be expected to cause a gradual decline in the overall intensities of these two spectral bands, which is not observed.

To test the second hypothesis of underestimation of the early-time coupling of HCN to the solvent bath, we carried out simulations as described in section 4.5.1 and the electronic supplementary information in which the force constant associated with the C−H stretching vibration of HCN was reduced, changing the computed vibrational frequency for this mode from 3468 cm^{-1} to 3155 cm^{-1} and then 3000 cm^{-1}. As is shown in the supplementary information, this reduction in vibrational frequency brings the HCN v_3 mode more closely into resonance with vibrational features evident in the computed spectrum of the THF solvent.

Fig. 12 shows the calculated relaxation of the total energy content in the v_3 mode in each of the three sets of simulations. The differences in relaxation timescales are dramatic. As the frequency of the v_3 band of HCN approaches that of the C−H stretching modes of THF, vibrational coupling between the THF solvent and HCN solute increases, and the decay time constant decreases. Fitting each of the curves in Fig. 12 yields energy decay time constants of 24 ps (single exponential fit for $v_3 \sim 3000$ cm^{-1}), 42 ps (single exponential fit for $v_3 \sim 3155$ cm^{-1}), and 15 and 400 ps (a double-exponential fit was required for $v_3 \sim 3468$ cm^{-1}). This outcome suggests that increasing the spectral overlap between the HCN and solvent modes gives an improved account of the experimental observations of production and fast vibrational relaxation of the HCN.

The combination of simulations and experiments therefore suggests extensive vibrational excitation of the nascent HCN from reaction (1), with the excitation localized in the C−H stretching mode in preference to the C≡N stretch. Rapid coupling of much of this initial excitation

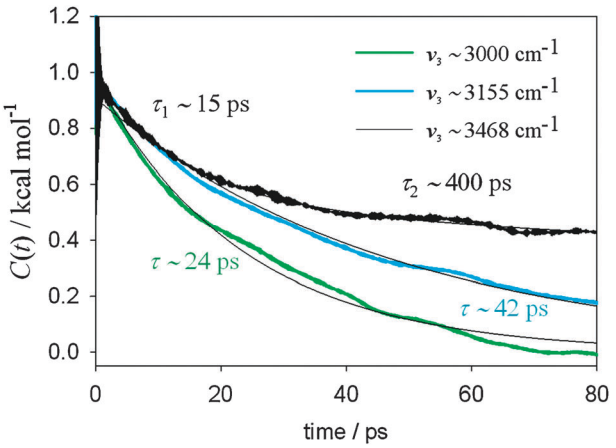

Fig. 12 Time dependent correlation functions and characteristic exponential decay timescales for the total energy content of the ν_3 mode of HCN in solution in THF. Each of the curves corresponds to simulations run using a different value for the H–CN force constant, resulting in the vibrational frequencies shown in the inset key and the HCN ν_3 fundamental bands shown in computed spectra in Fig. S2 of electronic supplementary information.

occurs to the surrounding bath on a timescale of $\sim$10 ps because of interaction of HCN(001) with near-resonant modes of THF.

5. Conclusions

The HCN products of reactions of CN radicals with THF (either the neat liquid or in solution in $CDCl_3$ or CD_2Cl_2) and the DCN products of CN radical reactions with liquid d_8-THF are shown by a combination of experimental measurements and molecular dynamics simulations to be formed with vibrational excitation in the ν_3 (C−H or C−D stretching) mode. A series of dilution experiments in which various concentrations of THF were employed in the range 0–4.5 M in $CDCl_3$ or CD_2Cl_2 demonstrate pseudo-first order kinetics for the production of HCN, and the analysis yields a bimolecular rate coefficient ($(1.57 \pm 0.12) \times 10^{10}$ M^{-1} s^{-1}) that agrees well with that for the gas-phase reaction of CN with ethane. The rate coefficients do not depend on the choice of $CDCl_3$ or CD_2Cl_2 as the solvent.

The observation of vibrationally excited HCN or DCN products echoes the outcomes of our study of CN radical reactions with cyclohexane and d_{12}-cyclohexane in a variety of chlorinated solvents, despite indications from IR spectra that the HCN (DCN) interacts more strongly with THF (or d_8-THF) than with cyclohexane or solvents such as chloroform. However, the relaxation of the nascent vibrational excitation occurs with time constants <10 ps in the presence of THF, compared to 265 ± 20 ps for cyclohexane/$CDCl_3$ solutions, consistent with a stronger coupling between the HCN and the THF (or DCN and d_8-THF). The degree of vibrational excitation is apparently less in the DCN products than was observed for d_{12}-cyclohexane reactions in chlorinated solvents, which would also point to modifications to the reaction energy surface and dynamics by the d_8-THF.

A contrast is thus drawn between the effects of chlorinated solvents and a representative ether solvent on the dynamics of a chemical reaction in solution. The THF (d_8-THF) is more strongly interacting with the HCN (DCN), as shown by the larger solvent shifts and greater broadening of vibrational bands, and the much shorter relaxation times to form ground state products. Nevertheless, this solvent coupling does not efficiently damp the vibrational excitation of the nascent products of bimolecular reactions of CN radicals with an organic co-reagent at shortest times after formation. It therefore seems likely that the effect of the interaction of the THF solvent molecules is greater with the reaction products than with the transient reacting species as they progress along the reaction coordinate.

Acknowledgements

We are grateful to Prof J.N. Harvey for many valuable discussions. The ULTRA laser complex at the Central Laser Facility, Rutherford Appleton Laboratory is funded by STFC and BBSRC (STFC Facility Grant ST/501784). The Bristol group gratefully acknowledges financial support from the EPSRC Programme Grant EP/G00224X. S.J.G. thanks the Leverhulme Trust for an Early Career Research Fellowship and EPSRC for a Career Acceleration Fellowship (EP/J002534/1), and A.J.O.E. thanks the Royal Society and the Wolfson Foundation for a Research Merit Award.

References

1 R. D. Levine, *Molecular Reaction Dynamics*, Cambridge University Press, Cambridge, 2005.
2 *Tutorials in Molecular Reaction Dynamics*, ed. M. Brouard and C. Vallance, Royal Society of Chemistry, Cambridge, 2010.
3 C. Waring, P. A. J. Bagot, M. L. Costen and K. G. McKendrick, *J. Phys. Chem. Lett.*, 2011, **2**, 12–18.
4 S. J. Greaves, R. A. Rose, T. A. A. Oliver, D. R. Glowacki, M. N. R. Ashfold, J. N. Harvey, I. P. Clark, G. M. Greetham, A. W. Parker, M. Towrie and A. J. Orr-Ewing, *Science*, 2011, **331**, 1423–1426.
5 D. R. Glowacki, A. J. Orr-Ewing and J. N. Harvey, *J. Chem. Phys.*, 2011, **134**, 204311.
6 D. R. Glowacki, R. A. Rose, S. J. Greaves, A. J. Orr-Ewing and J. N. Harvey, *Nat. Chem.*, 2011, **3**, 850–855.
7 A. J. Orr-Ewing, D. R. Glowacki, S. J. Greaves and R. A. Rose, *J. Phys. Chem. Lett.*, 2011, **2**, 1139–1144.
8 R. A. Rose, S. J. Greaves, T. A. A. Oliver, I. P. Clark, G. M. Greetham, A. W. Parker, M. Towrie and A. J. Orr-Ewing, *J. Chem. Phys.*, 2011, **134**, 244503.
9 D. Raftery, M. Iannone, C. M. Phillips and R. M. Hochstrasser, *Chem. Phys. Lett.*, 1993, **201**, 513–520.
10 D. Raftery, E. Gooding, A. Romanovsky and R. M. Hochstrasser, *J. Chem. Phys.*, 1994, **101**, 8572–8579.
11 L. Sheps, A. C. Crowther, C. G. Elles and F. F. Crim, *J. Phys. Chem. A*, 2005, **109**, 4296–4302.
12 L. Sheps, A. C. Crowther, S. L. Carrier and F. F. Crim, *J. Phys. Chem. A*, 2006, **110**, 3087–3092.
13 A. C. Crowther, S. L. Carrier, T. J. Preston and F. F. Crim, *J. Phys. Chem. A*, 2008, **112**, 12081–12089.
14 A. C. Crowther, S. L. Carrier, T. J. Preston and F. F. Crim, *J. Phys. Chem. A*, 2009, **113**, 3758–3764.
15 C. G. Elles and F. F. Crim, *Annu. Rev. Phys. Chem.*, 2006, **57**, 273–302.
16 D. T. Bowron, J. L. Finney and A. K. Soper, *J. Am. Chem. Soc.*, 2005, **128**, 5119–5126.
17 M. C. Larsen and B. J. Schwartz, *J. Chem. Phys.*, 2009, **131**, 154506.
18 W. J. Glover, R. E. Larsen and B. J. Schwartz, *J. Chem. Phys.*, 2010, **132**, 144102.

19 A. E. Bragg and B. J. Schwartz, *J. Phys. Chem. B*, 2008, **112**, 483–494.
20 G. M. Greetham, P. Burgos, Q. Cao, I. P. Clark, P. S. Codd, R. C. Farrow, M. W. George, M. Kogimitzis, P. Matousek, A. W. Parker, M. R. Pollard, D. A. Robinson, Z. J. Xin and M. Towrie, *Appl. Spectrosc.*, 2010, **64**, 1311.
21 W. Hess and S. R. Leone, *J. Chem. Phys.*, 1987, **86**, 3773–3780.
22 A. E. Douglas and D. Sharma, *J. Chem. Phys.*, 1953, **21**, 448–458.
23 H.-J. Werner, P. J. Knowles, R. Lindh, F. R. Manby, M. Schütz, P. Celani, T. Korona, G. Rauhut, R. D. Amos, A. Bernhardsson, A. Berning, D. L. Cooper, M. J. O. Deegan, A. J. Dobbyn, F. Eckert, C. Hampel, G. Hetzer, A. W. Lloyd, S. J. McNicholas, W. Meyer, M. E. Mura, A. Nicklass, P. Palmieri, R. Pitzer, U. Schumann, H. Stoll, A. J. Stone and R. Tarroni, *MOLPRO, version 2006.1*, a package of *ab initio* programs, see www.molpro.net.
24 D. F. McMillen and D. M. Golden, *Annu. Rev. Phys. Chem.*, 1982, **33**, 493–532.
25 A. G. Maki and R. L. Sams, *J. Chem. Phys.*, 1981, **75**, 4178–4182.
26 W. P. Hess, J. L. Durant and F. P. Tully, *J. Phys. Chem.*, 1989, **93**, 6402–6407.
27 Y. Georgievskii and S. J. Klippenstein, *J. Phys. Chem. A*, 2007, **111**, 3802–3811.
28 A. M. Smith, S. L. Coy, W. Klemperer and K. K. Lehmann, *J. Mol. Spectrosc.*, 1989, **134**, 134–153.
29 U. Samuni, S. Kahana, R. Fraenkel, Y. Haas, D. Danovich and S. Shaik, *Chem. Phys. Lett.*, 1994, **225**, 391–397.
30 A. C. Moskun and S. E. Bradforth, *J. Chem. Phys.*, 2003, **119**, 4500–4515.
31 *NIST Chemistry Webbook, NIST Standard Reference Database Number 69*, ed. P. J. Linstrom and W. G. Mallard, Gaithersburg MD, p. 20899.
32 L. Herbert, I. W. M. Smith and R. D. Spencer-Smith, *Int. J. Chem. Kinet.*, 1992, **24**, 791.
33 R. J. Balla, K. H. Casleton, J. S. Adams and L. Pasternack, *J. Phys. Chem.*, 1991, **95**, 8694–8701.
34 B. R. Brooks, C. L. Brooks, III, A. D. Mackerell, Jr., L. Nilsson, R. J. Petrella, B. Roux, Y. Won, G. Archontis, C. Bartels, S. Boresch, A. Caflisch, L. Caves, Q. Cui, A. R. Dinner, M. Feig, S. Fischer, J. Gao, M. Hodoscek, W. Im, K. Kuczera, T. Lazaridis, J. Ma, V. Ovchinnikov, E. Paci, R. W. Pastor, C. B. Post, J. Z. Pu, M. Schaefer, B. Tidor, R. M. Venable, H. L. Woodcock, X. Wu, W. Yang, D. M. York and M. Karplus, *J. Comput. Chem.*, 2009, **30**, 1545–1614.
35 D. R. Glowacki, E. Paci and D. V. Shalashilin, *J. Phys. Chem. B*, 2009, **113**, 16603–16611.
36 D. R. Glowacki, E. Paci and D. V. Shalashilin, *J. Chem. Theory Comput.*, 2011, **7**, 1244–1252.
37 E. A. Coutsias, C. Seok and K. A. Dill, *J. Comput. Chem.*, 2005, **26**, 1663–1665.
38 G. R. Kneller, *J. Chem. Phys.*, 2008, **128**, 6.
39 K. N. Kudin and A. Y. Dymarsky, *J. Chem. Phys.*, 2005, **122**, 2.
40 *NIST Chemistry Webbook, NIST Standard Reference Database Number 69, in National Institute of Standards and Technology*, ed. P. J. Linstrom and W. G. Mallard, Gaithersburg MD, p. 20899.
41 R. M. Whitnell, K. R. Wilson and J. T. Hynes, *J. Chem.Phys.*, 1992, **96**, 5354–5369.